Quantum-classical reaction rate theory

G. Hanna, H. Kim, and R. Kapral

Chemical Physics Theory Group
Department of Chemistry, 80 St. George St.
University of Toronto, Toronto, Canada *M5S 3H6*
ghanna@chem.utoronto.ca
hkim@chem.utoronto.ca
rkapral@chem.utoronto.ca

Summary. A correlation function formalism for the calculation of rate constants in mixed quantum-classical systems is presented. The full quantum equilibrium density is retained in the rate expressions and quantum-classical Liouville dynamics is used to propagate the species variables in time. Results for a model two-level system coupled to a nonlinear oscillator that is coupled to a harmonic bath and for a proton transfer reaction in a polar liquid solvent are presented. The rate coefficients for these systems are computed using surface-hopping dynamics based on the solution of the quantum-classical Liouville equation.

Key words: quantum rate constants, quantum time correlation functions, quantum-classical Liouville dynamics, condensed phase reactions, proton transfer, two-level systems

1 Introduction

A knowledge of the rates of condensed phase chemical reactions is necessary for an understanding of many problems in chemistry and biology. If one is interested in the reactive dynamics of a light particle immersed in an environment of heavy molecules, a quantum rate theory is required to correctly describe this dynamics. Consider a proton transfer occurring in a solvent or large molecule. Due to its light mass, the proton's thermal deBroglie wavelength is comparable in length to the distance over which it travels. As a result, the proton must be treated quantum mechanically and the importance of such quantum effects is well documented. Experimental evidence suggests that hydrogen tunneling is important in enzyme catalysis under physiological conditions [1]. The magnitude of such quantum effects can be gauged by comparing the measured or calculated deuterium kinetic isotope effect for these reactions with that predicted by classical transition state theory. In addition, quantum effects in the environment surrounding the proton may be significant. Quantum phenomena exist in the solvent dynamics associated with the

transfer of excess protons in liquid water and can explain the anomalously high mobility of these protons [2, 3].

Although it is not difficult to write a correlation function expression for the time-dependent rate coefficient of a reacting quantum system [4], a full quantum dynamical simulation of a condensed phase system containing a large number of degrees of freedom is not computationally feasible. Calculations of rate constants for reactive processes occurring in many-body environments, which incorporate quantum effects, have been performed using a variety of computational techniques. The techniques used include influence-functional [5, 6] and real-time path integral methods [7, 8], methods based on the stochastic Schrödinger equation [9, 10], centroid dynamics [11], golden rule and Fokker-Planck formulations [12], mode coupling theories [13, 14], techniques based on the initial value representation [15, 16, 17, 18, 19, 20, 21, 22], mapping Hamiltonian methods [23, 24], nonadiabatic statistical methods [25], surface-hopping schemes [26, 27, 28, 29, 30], multi-configuration time-dependent Hartree methods [31, 32], and methods based on the quantum-classical Liouville equation [33, 34, 35, 36, 37, 38].

In this chapter, we consider systems for which a description in terms of quantum-classical dynamics is appropriate [37], i.e. systems in which a subset of the degrees of freedom are treated quantum mechanically while the dynamics of the remainder of the degrees of freedom can be adequately described by classical mechanics. We first derive expressions for the quantum mechanical rate coefficient of a general reaction $A \rightleftharpoons B$ and then obtain their quantum-classical analogs. Next, we consider the choice of a reaction coordinate and the specification of species variables used to monitor the progress of a quantum reaction and discuss the rate expressions which arise from such a choice. We apply this quantum-classical rate theory to a two-level quantum system coupled to a classical nonlinear oscillator which is in turn coupled to a classical harmonic bath, and to the more realistic situation of a proton transfer reaction occurring in a polar solvent.

2 Rate Theory

Quantum-classical expressions for rate coefficients have been derived [40, 41], and computed for model systems [40, 41, 42] and proton transfer reactions [43]. An alternate approach to the calculation of quantum transport properties was described recently [44, 45]. The starting point of this approach is the full quantum mechanical expression for a transport property; however, the evolution of dynamical variables is carried out in the quantum-classical limit. This scheme has the advantage that the full quantum mechanical equilibrium structure of the system, described by a spectral density function, is retained; only the quantum mechanical time evolution is replaced by quantum-classical time evolution. The calculation of the quantum equilibrium structure, although a difficult problem, is far more tractable than that of the quantum time evolu-

tion of a many-body system. Exact expressions for the reaction rate coefficient have been derived in this more general context [45]. In many cases, one may take advantage of convenient features of the system to make approximations which simplify the computation of these expressions. For each system, the most applicable reaction coordinate must be identified, along with the dynamical variables which characterize the microscopic species involved in the reaction.

In this section we shall derive a series of quantum mechanical expressions for the rate coefficient of a general interconversion reaction $A \rightleftharpoons B$ starting from the flux-flux quantum correlation function. By taking the quantum-classical limit of these expressions, we obtain formulas that can be computed using quantum-classical surface-hopping dynamics.

2.1 Quantum Mechanical Rate Expressions

For a quantum mechanical system in thermal equilibrium undergoing a transformation $A \rightleftharpoons B$, a rate constant k_{AB} may be calculated from the time integral of a flux-flux correlation function [46],

$$k_{AB} = \frac{1}{n_A^{eq}} \int_0^\infty dt \langle \hat{j}_A ; \hat{j}_B(t) \rangle = \frac{1}{\beta n_A^{eq}} \int_0^\infty dt \langle \frac{i}{\hbar} [\hat{j}_B(t), \hat{A}] \rangle \ , \tag{1}$$

where $\hat{A} = \hat{N}_A$ is the A species operator, n_A^{eq} is the equilibrium density of species A, $\hat{j}_A = \dot{\hat{A}} = (i/\hbar)[\hat{H}, \hat{A}]$ is the flux of $\hat{A}$ with Hamiltonian $\hat{H}$, with an analogous expression for $\hat{j}_B$, $[\cdot, \cdot]$ is the commutator and the angular brackets $\langle \hat{A}; \hat{B} \rangle = \frac{1}{\beta} \int_0^\beta d\lambda \langle e^{\lambda \hat{H}} \hat{A} e^{-\lambda \hat{H}} \hat{B} \rangle$ denote a Kubo transformed correlation function, with $\beta = (k_B T)^{-1}$. The equilibrium quantum canonical average is $\langle \cdots \rangle = Z_Q^{-1} \mathrm{Tr} \cdots e^{-\beta \hat{H}}$, where Z_Q is the partition function. The time evolution of the reactive flux is given by projected dynamics. In simulations it is often convenient to consider the time-dependent rate coefficient defined as the finite time integral of the flux-flux correlation function,

$$\begin{aligned} k_{AB}(t) &= \frac{1}{n_A^{eq}} \int_0^t dt' \langle \hat{j}_A ; \hat{j}_B(t') \rangle = \frac{1}{n_A^{eq}} \langle \dot{\hat{A}} \, ; \hat{B}(t) \rangle \\ &= \frac{1}{\beta n_A^{eq}} \langle \frac{i}{\hbar} [\hat{B}(t), \hat{A}] \rangle \ , \end{aligned} \tag{2}$$

where we have replaced projected dynamics by ordinary dynamics and assumed $[\hat{B}, \hat{A}] = 0$.

Writing the second equality in Eq. (2) in detail and inserting arbitrary time variables t_1 and t_2, we can write the rate coefficient $k_{AB}(t)$ as,

$$k_{AB}(t) = \frac{1}{n_A^{eq} \beta Z_Q} \int_0^\beta d\lambda \mathrm{Tr} \Big(\dot{\hat{A}}(t_1 - i\hbar\lambda) e^{\frac{i}{\hbar}\hat{H}t'} \hat{B}(t_2) e^{-\frac{i}{\hbar}\hat{H}t'} e^{-\beta \hat{H}} \Big) \ , \tag{3}$$

where $t' \equiv t + t_1 - t_2$. To insert the times t_1 and t_2, we used the fact that the time evolution of an operator $\hat{O}$ is given by $\hat{O}(t) = e^{\frac{i}{\hbar}\hat{H}t}\hat{O}e^{-\frac{i}{\hbar}\hat{H}t}$.

We partition the entire quantum system into a subsystem $\mathcal{S}$ plus environment $\mathcal{E}$ so that the Hamiltonian is the sum of the kinetic energy operators of the subsystem and environment and the potential energy of the entire system, $\hat{H} = \hat{P}^2/2M + \hat{p}^2/2m + \hat{V}(\hat{q}, \hat{Q})$, where lower and upper case symbols refer to the subsystem and environment, respectively. In the next subsection we shall show how the rate coefficients for a system partitioned in this way can be evaluated in the quantum-classical limit. For the present, however, it is convenient to first make a Wigner transform over all degrees of freedom, subsystem plus environment, and later single out the subsystem and environmental degrees of freedom for different treatments. Introducing a coordinate representation $\{\mathcal{Q}\} = \{q\}\{Q\}$ of the operators in Eq. (3) (calligraphic symbols denote variables for the entire system), making the change of variables $\mathcal{Q}_1 = \mathcal{R}_1 - \mathcal{Z}_1/2$, $\mathcal{Q}_2 = \mathcal{R}_1 + \mathcal{Z}_1/2$, etc., and then expressing the matrix elements of the operators in terms of their Wigner transforms, we obtain

$$\begin{aligned} k_{AB}(t) = \frac{1}{\beta n_A^{eq}} \int_0^\beta d\lambda \int d\mathcal{X}_1 d\mathcal{X}_2 (\dot{A})_W(\mathcal{X}_1, t_1) B_W(\mathcal{X}_2, t_2) \\ \times \frac{1}{(2\pi\hbar)^{2\nu} Z_Q} \int d\mathcal{Z}_1 d\mathcal{Z}_2 e^{-\frac{i}{\hbar}(\mathcal{P}_1\cdot\mathcal{Z}_1 + \mathcal{P}_2\cdot\mathcal{Z}_2)} \\ \times \left\langle \mathcal{R}_1 + \frac{\mathcal{Z}_1}{2} \left| e^{\frac{i}{\hbar}\hat{H}(t'+i\hbar\lambda)} \right| \mathcal{R}_2 - \frac{\mathcal{Z}_2}{2} \right\rangle \\ \times \left\langle \mathcal{R}_2 + \frac{\mathcal{Z}_2}{2} \left| e^{-\beta\hat{H} - \frac{i}{\hbar}\hat{H}(t'+i\hbar\lambda)} \right| \mathcal{R}_1 - \frac{\mathcal{Z}_1}{2} \right\rangle, \end{aligned} \tag{4}$$

where $Z_Q = (2\pi\hbar)^{-\nu} \int d\mathcal{X} (e^{-\beta\hat{H}})_W(\mathcal{X})$. In writing this equation we used the fact that the matrix element of an operator $\hat{O}(t)$ can be expressed in terms of its Wigner transform $O_W(\mathcal{X}, t)$ as

$$\left\langle \mathcal{R} - \frac{\mathcal{Z}}{2} \left| \hat{O}(t) \right| \mathcal{R} + \frac{\mathcal{Z}}{2} \right\rangle = \frac{1}{(2\pi\hbar)^\nu} \int d\mathcal{P} e^{-\frac{i}{\hbar}\mathcal{P}\cdot\mathcal{Z}} O_W(\mathcal{X}, t), \tag{5}$$

where ν is the coordinate space dimension and

$$O_W(\mathcal{X}, t) = \int d\mathcal{Z} e^{\frac{i}{\hbar}\mathcal{P}\cdot\mathcal{Z}} \left\langle \mathcal{R} - \frac{\mathcal{Z}}{2} \left| \hat{O}(t) \right| \mathcal{R} + \frac{\mathcal{Z}}{2} \right\rangle , \tag{6}$$

defines the Wigner transform. We use the notation $\mathcal{R} = (r, R)$, $\mathcal{P} = (p, P)$ and $\mathcal{X} = (r, R, p, P)$, where again the lower case symbols refer to the subsystem and the upper case symbols refer to the environment.

We define the spectral density by

$$W(\mathcal{X}_1, \mathcal{X}_2, t) = \frac{1}{(2\pi\hbar)^{2\nu} Z_Q} \int d\mathcal{Z}_1 d\mathcal{Z}_2 e^{-\frac{i}{\hbar}(\mathcal{P}_1\cdot\mathcal{Z}_1 + \mathcal{P}_2\cdot\mathcal{Z}_2)}$$

$$\times \left\langle \mathcal{R}_1 + \frac{\mathcal{Z}_1}{2} \left| e^{\frac{i}{\hbar}\hat{H}t} \right| \mathcal{R}_2 - \frac{\mathcal{Z}_2}{2} \right\rangle$$
$$\times \left\langle \mathcal{R}_2 + \frac{\mathcal{Z}_2}{2} \left| e^{-\beta\hat{H} - \frac{i}{\hbar}\hat{H}t} \right| \mathcal{R}_1 - \frac{\mathcal{Z}_1}{2} \right\rangle . \quad (7)$$

If we let

$$\overline{W}(\mathcal{X}_1, \mathcal{X}_2, t) = \frac{1}{\beta}\int_0^\beta d\lambda W(\mathcal{X}_1, \mathcal{X}_2, t + i\hbar\lambda) \quad (8)$$
$$= \frac{2}{\beta}\int_0^{\frac{\beta}{2}} d\lambda \mathrm{Re}W(\mathcal{X}_1, \mathcal{X}_2, t + i\hbar\lambda),$$

we can write the rate coefficient as

$$k_{AB}(t) = \frac{1}{n_A^{eq}}\int d\mathcal{X}_1 d\mathcal{X}_2 (\dot{A})_W(\mathcal{X}_1, t_1) B_W(\mathcal{X}_2, t_2)\overline{W}(\mathcal{X}_1, \mathcal{X}_2, t + t_1 - t_2) \quad (9)$$

We may choose the times t_1 and t_2 to yield various forms for the correlation function. Since the time evolution of the operator is usually more convenient than that of the spectral density, we set $t_1 = 0$ and $t_2 = t$ to give

$$k_{AB}(t) = \frac{1}{n_A^{eq}}\int d\mathcal{X}_1 d\mathcal{X}_2 (iL_W(\mathcal{X}_1)A_W(\mathcal{X}_1))B_W(\mathcal{X}_2, t)\overline{W}(\mathcal{X}_1, \mathcal{X}_2, 0) \; . \quad (10)$$

The quantum Liouville operator in Wigner-transformed form is $iL_W = \frac{2}{\hbar}H_W(\mathcal{X})\sin\left(\frac{\hbar\Lambda}{2}\right)$, where Λ is the negative of the Poisson bracket operator. We can rewrite Eq. (10) as

$$k_{AB}(t) = \frac{1}{n_A^{eq}}\int d\mathcal{X} B_W(\mathcal{X}, t)\overline{W}_{A'}(\mathcal{X}, 0), \quad (11)$$

where [1]

$$\overline{W}_{A'}(\mathcal{X}, t) = \int d\mathcal{X}' (iL_W(\mathcal{X}')A_W(\mathcal{X}'))\overline{W}(\mathcal{X}', \mathcal{X}, t). \quad (12)$$

¿From the last equality in Eq. (2), we can obtain an alternative form of the rate coefficient involving the commutator of $\hat{A}$ and $\hat{B}(t)$. Performing a set of manipulations similar to those used above, we may show that $k_{AB}(t)$ is also given by

$$k_{AB}(t) = \frac{i}{\hbar\beta n_A^{eq}}\int d\mathcal{X}_1 d\mathcal{X}_2 A_W(\mathcal{X}_1)B_W(\mathcal{X}_2, t)$$
$$\times [W(\mathcal{X}_1, \mathcal{X}_2, i\hbar\beta) - W(\mathcal{X}_1, \mathcal{X}_2, 0)]$$
$$= \frac{2}{\hbar\beta n_A^{eq}}\int d\mathcal{X}_1 d\mathcal{X}_2 A_W(\mathcal{X}_1)B_W(\mathcal{X}_2, t)\mathrm{Im}W(\mathcal{X}_1, \mathcal{X}_2, 0), \quad (13)$$

[1] Here, $\overline{W}_{A'}$ corresponds exactly to $\overline{W}_A$ defined in Ref. [47].

where Im stands for the imaginary part. Using the definition

$$W_A(\mathcal{X},t) = \int d\mathcal{X}' A_W(\mathcal{X}') W(\mathcal{X}',\mathcal{X},t), \tag{14}$$

we can rewrite $k_{AB}(t)$ as

$$k_{AB}(t) = \frac{2}{\hbar\beta n_A^{eq}} \int d\mathcal{X} B_W(\mathcal{X},t) \mathrm{Im} W_A(\mathcal{X},0). \tag{15}$$

So far, both Eqs. (11) and (15) for the time-dependent rate coefficient are exact.

We find that the following symmetry relations hold for W:

$$W(\mathcal{X}_1,\mathcal{X}_2,t)^* = W(\mathcal{X}_2,\mathcal{X}_1,-t)\ , \tag{16}$$

$$W(\mathcal{X}_1,\mathcal{X}_2,t+i\hbar\lambda)^* = W(\mathcal{X}_1,\mathcal{X}_2,t+i\hbar(\beta-\lambda))\ . \tag{17}$$

Note that $W(\mathcal{X}',\mathcal{X},t+i\hbar\lambda)$ is real only for $\lambda = \frac{\beta}{2}$; namely,

$$W(\mathcal{X}_1,\mathcal{X}_2,t+\frac{i\hbar\beta}{2})^* = W(\mathcal{X}_1,\mathcal{X}_2,t+\frac{i\hbar\beta}{2}). \tag{18}$$

This corresponds to the first order term when $\overline{W}$ is expanded in terms of β,

$$\overline{W}(\mathcal{X}_1,\mathcal{X}_2,0) = W(\mathcal{X}_1,\mathcal{X}_2,\frac{i\hbar\beta}{2}) + \mathcal{O}(\beta^2). \tag{19}$$

In the high temperature limit, the higher order terms in β become negligible. Note that the symmetry relations above also hold for $W_{A'}(\mathcal{X},t)$.

In the long time limit, the time-dependent rate coefficient, $k_{AB}(t)$, decays to zero. However, if there is a large difference between the time scales of the chemical reaction and the transient microscopic dynamics, the rate coefficient first decays to a plateau from which the rate constant can be extracted. If absorbing boundaries are introduced to prevent escape of the trajectory from the metastable states once they are reached from the barrier top, the rate coefficient will no longer decay to zero and will assume a constant value at long times. This can be achieved more rigorously by formulating the rate expressions using projection operator techniques [46].

2.2 Quantum-Classical Rate Expressions

In this section we show how to take the quantum-classical limit of the general expressions for the rate coefficient, which treat the system plus environment fully quantum mechanically. By taking the quantum-classical limit [37] of these expressions we can obtain rate coefficient expressions that are amenable to solution using surface-hopping methods. The computation of the initial

value of W is still a challenging problem but far less formidable than the solution of the time-dependent Schrödinger equation for the entire quantum system.

To make a connection with the surface-hopping representation of the solution of the quantum-classical Liouville equation [37], we first observe that $A_W(\mathcal{X})$ can be written as

$$A_W(\mathcal{X}) = \int dz\, e^{\frac{i}{\hbar}p\cdot z} < r - \frac{z}{2}|\hat{A}_W(X)|r + \frac{z}{2} > , \tag{20}$$

where $\hat{A}_W(X)$ is the *partial* Wigner transform of $\hat{A}$, defined as in Eq. (6), but with the transform taken only over the environmental degrees of freedom. The partial Wigner transform of the Hamiltonian is $\hat{H}_W = P^2/2M + \hat{p}^2/2m + \hat{V}_W(\hat{q}, R) \equiv P^2/2M + \hat{h}_W(R)$, where $\hat{h}_W(R)$ is the Hamiltonian of the subsystem in the fixed field of the environment. The adiabatic eigenstates are the solutions of the eigenvalue problem, $\hat{h}_W(R)|\alpha; R >= E_\alpha(R)|\alpha; R >$. We may now express $A_W(\mathcal{X})$ in the adiabatic basis to obtain,

$$A_W(\mathcal{X}) = \sum_{\alpha\alpha'} \int dz\, e^{\frac{i}{\hbar}p\cdot z} < r - \frac{z}{2}|\alpha; R > A_W^{\alpha\alpha'}(X) < \alpha'; R|r + \frac{z}{2} > , \tag{21}$$

where $A_W^{\alpha\alpha'}(X) =< \alpha; R|\hat{A}_W(X)|\alpha'; R >$.

Inserting this expression and its analog for $B_W(\mathcal{X}_2)$ into Eq. (10), we obtain

$$k_{AB}(t) = \frac{1}{n_A^{eq}} \sum_{\alpha\alpha'} \int dX B_W^{\alpha\alpha'}(X, t) W_{A'}^{\alpha'\alpha}(X, \frac{i\hbar\beta}{2}), \tag{22}$$

using the approximation prescribed by Eq. (19). The matrix elements of $W_{A'}$ in the adiabatic basis are given by

$$W_{A'}^{\alpha'\alpha}(X, \frac{i\hbar\beta}{2}) = \sum_{\alpha_1\alpha_1'} \int dX' \Big(i\mathcal{L}(X') A_W(X') \Big)^{\alpha_1\alpha_1'} W^{\alpha_1'\alpha_1\alpha'\alpha}(X', X, \frac{i\hbar\beta}{2}), \tag{23}$$

where

$$\begin{aligned} W^{\alpha_1'\alpha_1\alpha'\alpha}(X', X, \frac{i\hbar\beta}{2}) &= \frac{1}{(2\pi\hbar)^{2\nu} Z_Q} \int dZ dZ' e^{-\frac{i}{\hbar}(P\cdot Z + P'\cdot Z')} \\ &\times < \alpha'; R| < R + \frac{Z}{2}|e^{-\frac{\beta}{2}\hat{H}}|R' - \frac{Z'}{2} > |\alpha_1; R' > \\ &\times < \alpha_1'; R'| < R' + \frac{Z'}{2}|e^{-\frac{\beta}{2}\hat{H}}|R - \frac{Z}{2} > |\alpha; R > . \end{aligned} \tag{24}$$

¿From Eq. (15), the alternative form of the rate coefficient can be obtained

$$k_{AB}(t) = \frac{2}{\hbar\beta n_A^{eq}} \sum_{\alpha\alpha'} \int d\mathcal{X} \mathrm{Im}[B_W^{\alpha\alpha'}(X,t) W_A^{\alpha'\alpha}(X,0)], \tag{25}$$

where

$$W_A^{\alpha'\alpha}(X,0) = \sum_{\alpha_1\alpha_1'} \int dX' A_W^{\alpha_1\alpha_1'}(X') W^{\alpha_1'\alpha_1\alpha'\alpha}(X',X,0). \tag{26}$$

In the quantum-classical limit, $B_W^{\alpha'\alpha}(X,t)$ satisfies the quantum-classical Heisenberg equation:

$$\frac{d}{dt} B_W^{\alpha'\alpha}(X,t) = \sum_{\beta\beta'} i\mathcal{L}_{\alpha'\alpha,\beta'\beta}(X) B_W^{\beta'\beta}(X,t). \tag{27}$$

The quantum-classical Liouville operator, $i\mathcal{L}$, in the adiabatic basis is given by $i\mathcal{L}_{\alpha\alpha',\beta\beta'}(X) = [i\omega_{\alpha\alpha'}(R) + iL_{\alpha\alpha'}(X)]\delta_{\alpha\beta}\delta_{\alpha'\beta'} - J_{\alpha\alpha',\beta\beta'}(X)$ [37], where the classical evolution operator is defined by

$$iL_{\alpha\alpha'} = \frac{P}{M}\frac{\partial}{\partial R} + \frac{1}{2}\left[F_W^{\alpha}(R) + F_W^{\alpha'}(R)\right]\frac{\partial}{\partial P}\,, \tag{28}$$

with

$$\begin{aligned} J_{\alpha\alpha',\beta\beta'}(X) = &-\frac{P}{M} d_{\alpha\beta}\left[1 + \frac{1}{2} S_{\alpha\beta}(R)\frac{\partial}{\partial P}\right]\delta_{\alpha'\beta'} \\ &- \frac{P}{M} d^*_{\alpha'\beta'}\left[1 + \frac{1}{2} S^*_{\alpha'\beta'}(R)\frac{\partial}{\partial P}\right]\delta_{\alpha\beta}. \end{aligned} \tag{29}$$

Here the frequency is $\omega_{\alpha\alpha'}(R) = [E_\alpha(R) - E_{\alpha'}(R)]/\hbar$, the Hellmann-Feynman force is $F_W^\alpha = -\left\langle \alpha; R \left| \partial \hat{V}_W(\hat{q},R)/\partial \hat{R} \right| \alpha; R \right\rangle$, the nonadiabatic coupling matrix element is $d_{\alpha\beta} = \langle \alpha; R | \nabla_R | \beta; R \rangle$, and $S_{\alpha\beta} = (E_\alpha - E_\beta) d_{\alpha\beta}[(P/M) \cdot d_{\alpha\beta}]^{-1}$.

It should be noted that $\overline{W}_{A'}^{\alpha'\alpha}(X,t)$ and $W_A^{\alpha'\alpha}(X,t)$ satisfy the following symmetry relations:

$$\overline{W}_{A'}^{\alpha'\alpha}(X,t)^* = \overline{W}_{A'}^{\alpha\alpha'}(X,t), \tag{30}$$

$$W_A^{\alpha'\alpha}(X, t + i\hbar\lambda)^* = W_A^{\alpha\alpha'}(X, t + i\hbar(\beta - \lambda)). \tag{31}$$

It follows that

$$\{\overline{W}_{A'}^{\alpha'\alpha}(X,t) + \overline{W}_{A'}^{\alpha\alpha'}(X,t)\}^* = \overline{W}_{A'}^{\alpha'\alpha}(X,t) + \overline{W}_{A'}^{\alpha\alpha'}(X,t), \tag{32}$$

and

$$\{W_A^{\alpha'\alpha}(X,t+i\hbar\lambda)+W_A^{\alpha\alpha'}(X,t+i\hbar\lambda)\}^* \\ = W_A^{\alpha'\alpha}(X,t+i\hbar(\beta-\lambda))+W_A^{\alpha\alpha'}(X,t+i\hbar(\beta-\lambda)). \quad (33)$$

Using these properties, we may write $k_{AB}(t)$ from Eqs. (22) and (25) as

$$k_{AB}(t)=\frac{1}{n_A^{eq}}\sum_\alpha\sum_{\alpha'\geq\alpha}(2-\delta_{\alpha'\alpha})\int dX\ \mathrm{Re}[B_W^{\alpha\alpha'}(X,t)W_{A'}^{\alpha'\alpha}(X,\frac{i\hbar\beta}{2})], \quad (34)$$

or

$$k_{AB}(t)=\frac{2}{\hbar\beta n_A^{eq}}\sum_\alpha\int dX\big(B_W^{\alpha\alpha}(X,t)\mathrm{Im}W_A^{\alpha\alpha}(X,0) \\ +\sum_{\alpha'>\alpha}\mathrm{Im}[B_W^{\alpha\alpha'}(X,t)\{W_A^{\alpha'\alpha}(X,0)-W_A^{\alpha\alpha'}(X,0)^*\}]\big). \quad (35)$$

These rate coefficient expressions involve quantum-classical evolution of the matrix element $B_W^{\alpha\alpha'}(X,t)$ but retain the full quantum equilibrium structure of the system. We now derive specific forms of the rate coefficient based on different choices of dynamical variables $B_W(X,t)$.

3 Species Variables

We now have to choose specific forms of the dynamical variables A_W and B_W which characterize the chemical species in the reacting mixture, but first we need some insight into how to choose them. This will be the topic of the next subsection.

3.1 Reaction Coordinate and Free Energy

To illustrate how one chooses a particular species variable, we consider a two-level quantum subsystem coupled to an environment with many degrees of freedom. This is an interesting case since many features of condensed phase proton and electron transfer processes can often be captured by such two-level models. In many situations, due to the nature of the coupling between the quantum and classical degrees of freedom, one may choose a reaction coordinate, $\xi(R)$, which depends solely (either directly or parametrically) on the classical coordinates. In such a case, reactive events in the quantum subsystem are reflected by changes in a function of the classical coordinates. The reaction coordinate must be appropriate in the sense that it will be able to detect the formation of the various chemical species in the reacting mixture, if monitored along the course of a reaction. The guide to the specification of the relevant species variables for our two-level model is provided by the structure of the ground and first excited state free energy profiles along $\xi(R)$.

The free energy along the reaction coordinate can be obtained analytically for simple two-level systems [40] or, more generally, generated from long constant temperature trajectories on the different adiabatic surfaces. The free energy corresponding to adiabatic surface α is given by

$$\beta W_\alpha(\xi') = -\ln \frac{P_\alpha(\xi')}{P_u}, \tag{36}$$

where P_u is the uniform probability density of ξ, and

$$P_\alpha(\xi') = \frac{\int dRdP\ \delta(\xi(R) - \xi')e^{-\beta H_\alpha}}{\sum_\alpha \int dRdP\ e^{-\beta H_\alpha}}\ , \tag{37}$$

is the probability density for finding the numerical value ξ' of $\xi(R)$ when the system is in adiabatic state α with Hamiltonian $H_\alpha = \sum_i P_i^2/(2M_i) + E_\alpha(R)$, where the sum runs over all classical particles i, and P_i and M_i are the momentum and mass of the i^{th} particle, respectively. We may then write the free energy as

$$\beta W_\alpha(\xi') = -\ln \frac{\langle \delta(\xi(R) - \xi')\rangle_\alpha}{P_u} - \ln \frac{p_\alpha}{p_1}\ , \tag{38}$$

where $\langle \delta(\xi(R) - \xi')\rangle_\alpha$ is defined by,

$$\langle \delta(\xi(R) - \xi')\rangle_\alpha = \frac{\int dRdP\ \delta(\xi(R) - \xi')e^{-\beta H_\alpha}}{\int dRdP\ e^{-\beta H_\alpha}}\ . \tag{39}$$

and can be estimated by binning $\xi(R)$ along a long trajectory on adiabatic surface α. The probability that the system is in state α is $p_\alpha = \int d\xi'\ P_\alpha(\xi')$, and therefore

$$\frac{p_\alpha}{p_1} = \frac{\int dRdPe^{-\beta(E_\alpha - E_1)}e^{-\beta H_1}}{\int dRdPe^{-\beta H_1}}\ . \tag{40}$$

This factor is related to the relative probability that the system is in state α (regardless of the value of ξ), and can be determined from a long adiabatic trajectory on the ground state surface.

Figure 1 schematically shows two sets of free energy profiles for a two-level system; they correspond to systems in which there is weak (left panel) and strong (right panel) coupling between the quantum subsystem and the reaction coordinate, respectively. In both, the ground state surface has two minima corresponding to two stable species separated by a high barrier at $\xi(R) = \xi^\ddagger$. In the left panel, the excited state surface is nearly parallel to the ground state surface, whereas in the right panel it has a single minimum. Since transitions between the two stable species will occur on a long time scale (due to the high barrier and excitations to higher states), we may identify the values of $\xi(R)$ greater than and less than $\xi^\ddagger$ with species A and B, respectively. Hence, we may use the Heaviside functions $\theta(\xi(R) - \xi^\ddagger)$ and $\theta(\xi^\ddagger - \xi(R))$ as variables which correspond to species A and B, respectively.

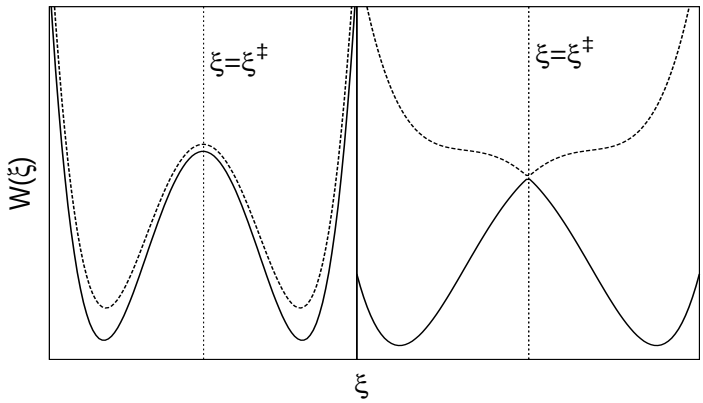

Fig. 1. A schematic illustration of two contrasting sets of free energy (W) profiles along a reaction coordinate ξ. The left and right panels respectively depict situations of weak and strong coupling between the quantum subsystem and reaction coordinate. The dotted lines at $\xi = \xi^{\ddagger}$ indicate the position of the barrier top.

Let us consider a system in which only one classical coordinate, R_0, is directly coupled to the quantum subsystem. In this case, the progress of the quantum reaction can be simply monitored by the reaction coordinate $\xi(R) = R_0$. For the remainder of this section, all the derivations are carried out using this reaction coordinate because the mathematical manipulations are less cumbersome using this reaction coordinate.

3.2 Reactive Flux Operator

The A and B species operators may be defined as $\hat{A}_W = \theta(-R_0)$ and $\hat{B}_W = \theta(R_0)$, where θ is the Heaviside function and the dividing surface is located at $\xi^{\ddagger} = 0$. For this choice of species variable, $W_{A'}^{\alpha'\alpha}(X, \frac{i\hbar\beta}{2})$ defined in Eq. (23), can be simplified by taking advantage of the fact that integrations over all X' coordinates can be performed to obtain,

$$
\begin{aligned}
W_{A'}^{\alpha'\alpha}(X, \frac{i\hbar\beta}{2}) = \frac{1}{(2\pi\hbar)^{\nu} Z_Q} \frac{i\hbar}{M_0} \int dZ dZ_0' (\partial\delta(Z_0')/\partial Z_0') e^{-\frac{i}{\hbar} P \cdot Z} \\
\times < \alpha'; R_0 | \left\langle R + \frac{Z}{2} \left| e^{-\frac{\beta}{2}\hat{H}} \right| - \frac{Z_0'}{2} \right\rangle \\
\times \left\langle \frac{Z_0'}{2} \left| e^{-\frac{\beta}{2}\hat{H}} \right| R - \frac{Z}{2} \right\rangle | \alpha; R_0 > . \qquad (41)
\end{aligned}
$$

In this equation the adiabatic eigenstates depend parametrically only on R_0 since the subsystem $\mathcal{S}$ couples directly only to the coordinate R_0.

In order to compute the rate, we need to carry out quantum-classical evolution of $B_W^{\alpha\alpha'}(X,t)$, as dictated by Eq. (27), and sample from an initial quantum distribution with weights determined by $W_{A'}^{\alpha'\alpha}(X,\frac{i\hbar\beta}{2})$. The imaginary time propagators in $W_{A'}^{\alpha'\alpha}(X,\frac{i\hbar\beta}{2})$ can, in principle, be computed using quantum path integral methods [48] or approximations such as linearization methods [23, 24, 49, 50]. Below we show how one may construct approximate analytical expressions for this quantity, which will be used to obtain the numerical results in the next section.

Parabolic potential in barrier region

In activated rate processes a knowledge of the dynamics of a system in the vicinity of its potential energy barrier is crucial for the calculation of the rate constant. In many situations the potential is locally parabolic in the barrier region and such harmonic barrier approximations have been employed frequently in the study of quantum and classical reaction rates [17, 51, 52, 53, 54, 55]. Here we show how the local harmonic character of the barrier along the reaction coordinate R_0 can be exploited to construct an approximate form for $W_A^{\alpha'\alpha}(X,\frac{i\hbar\beta}{2})$, which is useful for the situation depicted in the left panel of Fig. 1.

To proceed with the analytical calculation, we first partition the Hamiltonian into $\hat{H}=\hat{H}_{sn}+\hat{H}_{b(n)}$, where $\hat{H}_{sn}=\hat{H}_s+\hat{H}_n+\hat{V}_{sn}$ is the Hamiltonian of the subsystem plus a subset of degrees of freedom $\mathcal{N}$ plus the coupling between them, and $\hat{H}_{b(n)}$ is the Hamiltonian of the bath $\mathcal{B}$ in the field of $\mathcal{N}$. For our model the subset $\mathcal{N}$ is just that associated with the R_0 coordinate. Then, we assume that the imaginary time propagator may be written as $\exp(-\beta\hat{H}/2)\approx\exp(-\beta\hat{H}_{sn}/2)\exp(-\beta\hat{H}_{b(n)}/2)$, so that Eq. (41) for $W_{A'}^{\alpha'\alpha}(X,\frac{i\hbar\beta}{2})$ is given by

$$\begin{aligned} W_{A'}^{\alpha'\alpha}(X,\frac{i\hbar\beta}{2}) &= \frac{1}{Z_Q}\frac{i}{2\pi M_0}\int dZ_0 dZ_0' \delta'(Z_0') e^{-\frac{i}{\hbar}P_0\cdot Z_0} \\ &\times <\alpha';R_0|\left\langle R_0+\frac{Z_0}{2}\left|e^{-\frac{\beta}{2}\hat{H}_{sn}}\right|-\frac{Z_0'}{2}\right\rangle \\ &\times\left\langle\frac{Z_0'}{2}\left|e^{-\frac{\beta}{2}\hat{H}_{sn}}\right|R_0-\frac{Z_0}{2}\right\rangle|\alpha;R_0>\rho_b(P_b,R_b;R_0), \end{aligned} \tag{42}$$

where $\rho_b(P_b,R_b;R_0)$ is proportional to the Wigner transform of the canonical equilibrium density matrix for the bath in the field of the R_0 coordinates,

$$\begin{aligned} \rho_b(P_b,R_b;R_0) &= \frac{1}{(2\pi\hbar)^{\nu-1}}\int dZ_b e^{-\frac{i}{\hbar}P_b\cdot Z_b} \\ &\times\left\langle R_b+\frac{Z_b}{2}\left|e^{-\beta\hat{H}_{b(n)}}\right|R_b-\frac{Z_b}{2}\right\rangle. \end{aligned} \tag{43}$$

Next, we single out the barrier region around $R_0 = 0$ for special consideration. Separating the Hamiltonian $\hat{H}_{sn}$ into a harmonic term $\hat{H}_{h0} = P_0^2/2M_0 - \frac{1}{2}M_0\omega^{\ddagger 2}R_0^2$ (where $\omega^{\ddagger}$ is the frequency at the barrier top) and remainder terms $\hat{h}_{sn}$, we can write $\hat{H}_{sn} = \hat{H}_{h0} + \hat{h}_{sn}$. The eigenstates of $\hat{h}_{sn}$ are $|\alpha; R_0>$ as above but the eigenvalues, denoted by $\varepsilon_\alpha(R_0)$, are related to the $E_\alpha(R_0)$ introduced earlier by $\varepsilon_\alpha(R_0) = E_\alpha(R_0) + \frac{1}{2}M_0\omega^{\ddagger 2}R_0^2$. Taking $\exp(-\beta\hat{H}_{sn}/2) \approx \exp(-\beta\hat{H}_{h0}/2)\exp(-\beta\hat{h}_{sn}/2)$, the matrix elements in Eq. (42) can then be written as

$$
\begin{aligned}
&< \alpha'; R_0| < R_0 + \frac{Z_0}{2}|e^{-\frac{\beta}{2}\hat{H}_{sn}}| - \frac{Z_0'}{2} >< \frac{Z_0'}{2}|e^{-\frac{\beta}{2}\hat{H}_{sn}}|R_0 - \frac{Z_0}{2} > |\alpha; R_0> \\
&=< R_0 + \frac{Z_0}{2}|e^{-\frac{\beta}{2}\hat{H}_{h0}}| - \frac{Z_0'}{2} >< \frac{Z_0'}{2}|e^{-\frac{\beta}{2}\hat{H}_{h0}}|R_0 - \frac{Z_0}{2} > \\
&\quad \times < \alpha'; R_0|e^{-\frac{\beta}{2}\hat{h}_{sn}(R_0+\frac{Z_0}{2})}e^{-\frac{\beta}{2}\hat{h}_{sn}(R_0-\frac{Z_0}{2})}|\alpha; R_0> . \qquad (44)
\end{aligned}
$$

Using the representation of $\hat{h}_{sn}$ in the adiabatic basis, $e^{-\frac{\beta}{2}\hat{h}_{sn}(R_0)} = \sum_\alpha |\alpha; R_0> e^{-\frac{\beta}{2}\varepsilon_\alpha(R_0)} < \alpha; R_0|$, expressing the matrix element in a Taylor series in Z_0 and retaining up to first order terms in Z_0, we find

$$
\begin{aligned}
&< \alpha'; R_0|e^{-\frac{\beta}{2}h_{sn}(R_0+\frac{Z_0}{2})}e^{-\frac{\beta}{2}h_{sn}(R_0-\frac{Z_0}{2})}|\alpha; R_0> \\
&\quad = e^{-\beta\varepsilon_\alpha(R_0)}\left[\delta_{\alpha\alpha'} + \frac{Z_0}{2}O_{\alpha'\alpha}(R_0)d_{\alpha'\alpha}(R_0) + \mathcal{O}(Z_0^2)\right], \qquad (45)
\end{aligned}
$$

where $O_{\alpha'\alpha}(R_0) = \left(1 - e^{-\frac{\beta}{2}\varepsilon_{\alpha'\alpha}(R_0)}\right)^2$ and $\varepsilon_{\alpha'\alpha} = \varepsilon_{\alpha'} - \varepsilon_\alpha$.

Finally, using the expression for the matrix elements of the harmonic oscillator imaginary time propagator,

$$
\begin{aligned}
< R_0|e^{-\frac{\beta}{2}\hat{H}_{h0}}|R_0'> &= \sqrt{\frac{2aM_0u}{\pi\sin u}}\exp[-aM_0u \\
&\{-(R_0+R_0')^2\tan\frac{u}{2} + (R_0-R_0')^2\cot\frac{u}{2}\}], \qquad (46)
\end{aligned}
$$

where $u = \beta\hbar\omega^{\ddagger}/2$ and $a = (2\beta\hbar^2)^{-1}$, and carrying out the integrations over Z_0 and Z_0', we have

$$
\begin{aligned}
W_{A'}^{\alpha'\alpha}(X, \frac{i\hbar\beta}{2}) &= \frac{1}{2\pi\hbar Z_Q}\frac{1}{\cos^2 u}\sqrt{\frac{2M_0u'}{\beta\hbar^2\pi}}e^{-\frac{2M_0u'}{\beta\hbar^2}R_0^2} \\
&\quad \times\frac{P_0}{M_0}e^{-\frac{\beta P_0^2}{2M_0u'}}F_{\alpha'\alpha}(R_0)\rho_b(P_b, R_b; R_0), \qquad (47)
\end{aligned}
$$

where $u' \equiv u\cot u$ and

$$
F_{\alpha'\alpha}(R_0) = e^{-\beta\varepsilon_\alpha(R_0)}\left(\delta_{\alpha'\alpha} + \frac{1}{2}(1 - \frac{\beta P_0^2}{M_0u'})\frac{i\hbar}{P_0}d_{\alpha'\alpha}O_{\alpha'\alpha}\right). \qquad (48)
$$

The off-diagonal contribution to $W_{A'}$ is imaginary and therefore, from Eq. (34), only the imaginary part of $B_W^{\alpha\alpha'}(X,t)$ contributes to the rate.

Partitioning of the propagator

When the ground and excited states have different structures in the barrier region (as in the right panel of Fig. 1), the parabolic approximation used above is no longer valid and another approximation must be made. In this connection, instead of singling out the harmonic part of $\hat{H}_{sn}$ in the barrier region, one may partition $\hat{H}_{sn}$ into kinetic plus potential terms as $\hat{H}_{sn} = \hat{P}_0^2/2M_0 + \hat{h}_0$. Then approximating the propagator in Eq. (42) as $e^{\beta\hat{H}_{sn}/2} \approx e^{\beta\hat{P}_0^2/4M_0} e^{\beta\hat{h}_0/2}$, and carrying out a series of calculations similar to those outlined above, we obtain

$$W_{A'}^{\alpha'\alpha}(X, \frac{i\hbar\beta}{2}) = \frac{1}{2\pi\hbar Z_Q}\sqrt{\frac{2M_0}{\beta\hbar^2\pi}} e^{-\frac{2M_0}{\beta\hbar^2}R_0^2} \times \frac{P_0}{M_0} e^{-\frac{\beta P_0^2}{2M_0}} \mathcal{F}_{\alpha'\alpha}(R_0)\rho_b(P_b, R_b; R_0), \tag{49}$$

where $\mathcal{F}_{\alpha'\alpha}$ has a definition similar to that of $F_{\alpha'\alpha}$ but with $\varepsilon_\alpha(R_0)$ replaced by $E_\alpha(R_0)$,

$$\mathcal{F}_{\alpha'\alpha}(R_0) = e^{-\beta E_\alpha(R_0)} \left(\delta_{\alpha'\alpha} + \frac{1}{2}(1 - \frac{\beta P_0^2}{M_0})\frac{i\hbar}{P_0} d_{\alpha'\alpha}\mathcal{O}_{\alpha'\alpha}\right). \tag{50}$$

Likewise, $\mathcal{O}_{\alpha'\alpha}$ has a definition analogous to that of $O_{\alpha'\alpha}$ with $\varepsilon_\alpha(R_0)$ replaced by $E_\alpha(R_0)$.

The advantages of the two methods based on Eqs. (47) and (49) are worth noting. Equation (49) does not assume a particular form for the potential in the barrier region, while in Eq. (47), a harmonic form is assumed. However, Eq. (47) retains the quantum effects resulting from the coupling between the potential and kinetic terms unlike Eq. (49).

Classical treatment of environmental coordinates

Making the high temperature approximation $\lim_{\beta\to 0}\sqrt{\frac{a}{\beta\pi}} e^{-\frac{a}{\beta}R_0^2} = \delta(R_0)$ and using the classical analog of Eq. (43), $\rho_b^{cl}(P_b, R_b; R_0) = \frac{e^{-\beta H_{b(n)}}}{(2\pi\hbar)^{\nu-1}}$, Eq. (49) reduces to

$$\begin{aligned} W_{A'}^{\alpha'\alpha}(X, \frac{i\hbar\beta}{2}) &= \frac{1}{2\pi\hbar Z_Q}\delta(R_0)\frac{P_0}{M_0} e^{-\frac{\beta P_0^2}{2M_0}} \mathcal{F}_{\alpha'\alpha}(R_0)\rho_b^{cl}(P_b, R_b; R_0) \\ &= \frac{1}{(2\pi\hbar)^\nu Z_Q}\delta(R_0)\frac{P_0}{M_0} e^{-\beta H_\alpha(X)} \\ &\quad \times \left(\delta_{\alpha'\alpha} + \frac{1}{2}(1 - \frac{\beta P_0^2}{M_0})\frac{i\hbar}{P_0} d_{\alpha'\alpha}\mathcal{O}_{\alpha'\alpha}\right), \end{aligned} \tag{51}$$

where $H_\alpha(X) = H_{b(n)} + E_\alpha(R_0)$. This result may be substituted into Eq. (34) to obtain an expression for the rate coefficient:

$$k_{AB}(t) = k^d_{AB}(t) + k^o_{AB}(t), \tag{52}$$

where the diagonal contribution is

$$k^d_{AB}(t) = \frac{-1}{n^{eq}_A (2\pi\hbar)^\nu Z_Q} \sum_\alpha \int dX B^{\alpha\alpha}_W(X,t)\delta(R_0)\frac{P_0}{M_0} e^{-\beta H_\alpha(X)}, \tag{53}$$

and the off-diagonal contribution is

$$\begin{aligned} k^o_{AB}(t) = \frac{1}{n^{eq}_A (2\pi\hbar)^\nu Z_Q} \sum_{\alpha'>\alpha} \int dX \mathrm{Im}\{B^{\alpha\alpha'}_W(X,t)\}\delta(R_0)\frac{P_0}{M_0} e^{-\beta H_\alpha(X)} \\ \times(1 - \frac{\beta P_0^2}{M_0})\frac{\hbar}{P_0} d_{\alpha'\alpha}\mathcal{O}_{\alpha'\alpha}. \end{aligned} \tag{54}$$

The diagonal contribution agrees with the result obtained earlier using quantum-classical linear response theory [40], while the off-diagonal contribution does not due to the inherent differences in the approximations made. For a general reaction coordinate, $\xi(R)$, the high temperature approximation leads to

$$\begin{aligned} k^d_{AB}(t) = \frac{-1}{n^{eq}_A (2\pi\hbar)^\nu Z_Q} \sum_\alpha \int dX \ \frac{P}{M} \cdot \nabla_R \xi(R) B^{\alpha\alpha}_W(X,t) \\ \times\delta(\xi(R) - \xi^\ddagger) e^{-\beta H_\alpha(X)} \ , \end{aligned} \tag{55}$$

and

$$\begin{aligned} k^o_{AB}(t) = \frac{1}{n^{eq}_A (2\pi\hbar)^\nu Z_Q} \sum_{\alpha'>\alpha} \int dX \mathrm{Im}\{B^{\alpha\alpha'}_W(X,t)\}\delta(\xi(R) - \xi^\ddagger) e^{-\beta H_\alpha(X)} \\ \times\Big(\sum_j \frac{\nabla_{R_j}\xi(R)}{M_j} \big[d^j_{\alpha'\alpha} - \beta P_j \big(\frac{P}{M} \cdot d_{\alpha'\alpha} \big) \big] \Big) \hbar \mathcal{O}_{\alpha'\alpha}. \end{aligned} \tag{56}$$

4 Applications

In order to compute the rate constants of processes such as proton and electron transport in condensed phases, one must account for the effects of the environmental degrees of freedom. The theory presented in the previous sections provides a convenient framework in which a rate study of such systems can be performed.

In this section, we show the results of a rate coefficient calculation for a proton transfer reaction occurring in a linear hydrogen-bonded complex dissolved in a polar solvent. The proton is treated quantum mechanically and the remainder of the degrees of freedom is treated classically. Valuable insight into

such rate processes can also be obtained, more efficiently, by studying simple transfer reaction models which simulate the effect of a condensed phase environment on a reaction coordinate. In this connection, we first show rate results for a two-level quantum system coupled to a classical nonlinear oscillator that is in turn coupled to classical harmonic bath. For these two applications, an appropriate choice of reaction coordinate and species variables is made and quantum-classical Liouville dynamics is used to evolve the species variables.

4.1 Two-level model for transfer reactions

Spin-boson-type models, where a two-level quantum system is bilinearly coupled to a bath of independent harmonic oscillators, have often been used to compute nonadiabatic reaction rates [8, 16, 23, 48, 56, 57]. For such spin-boson systems quantum-classical dynamics is exact and our simulation algorithms that employ quantum-classical trajectories have been shown [58] to reproduce the exact quantum results [56]. The rate constant for such spin-boson systems, when computed using quantum-classical dynamics and sampling from quantum initial states, corresponds to that obtained in a full quantum treatment [45, 47]. Here we consider a more complex model involving coupling between the two-level system, a nonlinear oscillator and a bath of harmonic oscillators as a more realistic model for quantum particle transfer in the condensed phase. No exact results are available for this model.

Model

The model system we consider has the Hamiltonian operator, expressed in the diabatic basis $\{|L\rangle, |R\rangle\}$ [40]

$$\mathbf{H} = \begin{pmatrix} V_n(R_0) + \hbar\gamma_0 R_0 & -\hbar\Omega \\ -\hbar\Omega & V_n(R_0) - \hbar\gamma_0 R_0 \end{pmatrix} + \left(\frac{P_0^2}{2M_0} + \sum_{j=1}^{N} \frac{P_j^2}{2M_j} + \sum_{j=1}^{N} \frac{M_j}{2}\omega_j^2 \left(R_j - \frac{c_j}{M_j\omega_j^2} R_0 \right)^2 \right) \mathbf{I} \,. \tag{57}$$

In this model, a two-level system is coupled to a classical nonlinear oscillator with mass M_0 and phase space coordinates (R_0, P_0). This coupling is given by $\hbar\gamma_0 R_0 = \hbar\gamma(R_0)$. The nonlinear oscillator, which has a quartic potential energy function $V_n(R_0) = aR_0^4/4 - M_0\omega^{\ddagger 2}R_0^2/2$, is then bilinearly coupled to a bath of N independent harmonic oscillators. From the first matrix in Eq. (57), we see that the diabatic energies are given by $E_{1,2}^d(R_0) = V_n(R_0) \pm \hbar\gamma_0 R_0$ and the coupling between the diabatic states is $-\hbar\Omega$. The bath harmonic oscillators labelled $j = 1, ..., N$ have masses M_j and frequencies ω_j. The bilinear coupling is characterized by an Ohmic spectral density

[56, 57], $J(\omega) = \pi \sum_{j=1}^{N} (c_j^2/(2M_j\omega_j^2))\delta(\omega - \omega_j)$, where $c_j = (\xi\hbar\omega_0 M_j)^{1/2}\omega_j$, $\omega_j = -\omega_c \ln(1 - j\omega_0/\omega_c)$ and $\omega_0 = \frac{\omega_c}{N}\left(1 - e^{-\omega_{max}/\omega_c}\right)$, with ω_c a cut-off frequency.

The adiabatic states obtained from the diagonalization of Hamiltonian (57) are given by

$$\begin{aligned} |1; R_0\rangle &= \frac{1}{\mathcal{N}}\left[(1+G)|L\rangle + (1-G)|R\rangle\right] \\ |2; R_0\rangle &= \frac{1}{\mathcal{N}}\left[-(1-G)|L\rangle + (1+G)|R\rangle\right], \end{aligned} \tag{58}$$

where $\mathcal{N}(R_0) = \sqrt{2(1+G^2(R_0))}$ and

$$G(R_0) = \gamma(R_0)^{-1}\left[-\Omega + \sqrt{\Omega^2 + \gamma^2(R_0)}\right]. \tag{59}$$

The corresponding adiabatic energies are $E_{1,2}(R) = V_b(R) \mp \sqrt{\Omega^2 + \gamma^2(R_0)}$, where

$$V_b(R) = V_n(R_0) + \sum_{j=0}^{N} \frac{P_j^2}{2M_j} + \sum_{j=1}^{N} \frac{M_j}{2}\omega_j^2 \left(R_j^2 - \frac{c_j}{M_j\omega_j^2}R_0\right)^2. \tag{60}$$

Insight into the nature of the quantum reaction dynamics can be gained by considering the ground and first excited adiabatic free energies along the R_0 coordinate, as given by

$$\begin{aligned} W_\alpha(R_0) &= -\beta^{-1} \ln\left(\int \prod_{j=1}^{N} dR_j \; Z_\alpha^{-1} e^{-\beta E_\alpha(R)}\right) \\ &= \beta^{-1}\ln Z_\alpha + V_n(R_0) \mp \sqrt{\Omega^2 + \gamma_0^2 R_0^2}\,, \end{aligned} \tag{61}$$

where $Z_\alpha = \int dR \;\exp(-\beta E_\alpha(R))$ and $\alpha = 1, 2$. They are plotted in Fig. 1 for both a small (left) and large (right) value of γ_0. Based on the structure of these profiles, we may choose $\theta(R_0)$ and $\theta(-R_0)$ for the A and B species variables, respectively.

For small values of γ_0, the potential in the reactant region is approximately harmonic, making the ground and excited free energy surfaces nearly parallel. As a result, the partition function for the reactant state, $n_A^{eq} Z_Q$, can be approximated using the mean free energy surface and given by

$$(n_A^{eq} Z_Q)^{-1} \approx e^{\beta V_r} \sinh(\beta\hbar\omega_r/2) \prod_{j=1}^{N} 2\sinh(\beta\hbar\omega_j/2), \tag{62}$$

where ω_r is the frequency in the reactant well and V_r is the bare potential at the bottom of it. Using the high temperature form of Eq. (62) in the transition state theory ($t = 0^+$) form of Eq. (53) we obtain

$$k_{AB}^{TST} \approx \frac{\omega_r e^{\beta V_r}}{2\pi} \frac{e^{-\beta\Omega} + e^{\beta\Omega}}{2}, \tag{63}$$

which will be used to scale the results presented in the figures. When the coupling between the two-level system and the quartic oscillator is negligible, Ω is also negligible, and k_{AB}^{TST} becomes the well-known value of $\omega_r e^{\beta V_r}/2\pi$. In this regime, a symmetric oscillator has the frequency $\omega_r \approx \sqrt{2}\omega^{\ddagger}$. Using these results and Eqs. (34) and (47) for $k_{AB}(t)$, the transmission coefficient, $\kappa_{AB}(t) = k_{AB}(t)/k_{AB}^{TST}$, takes the form

$$\kappa_{AB}(t) = -\sum_{\alpha} \sum_{\alpha' \geq \alpha} (2 - \delta_{\alpha'\alpha}) \int dX \mathrm{Re}[B_W^{\alpha\alpha'}(X,t) w_{QRB}^{\alpha'\alpha}(X)], \tag{64}$$

where

$$\begin{aligned} w_{QRB}^{\alpha'\alpha}(X) = & \frac{2u}{\sin 2u} \frac{\sinh u_r}{u_r} \frac{P_0}{M_0} \sqrt{\frac{\pi M_0 \beta}{2u'}} \frac{F_{\alpha'\alpha}}{\sum_\alpha e^{-\beta\varepsilon_\alpha(0)}} \\ & \times G_a(R_0; \frac{2M_0 u'}{\beta\hbar^2}) G_a(P_0; \frac{\beta}{2M_0 u'}) \\ & \times \prod_{j=1}^{N} G_a(R_j - \frac{c_j R_0}{M_j\omega_j^2}; \frac{\beta}{2u_j''} M_j\omega_j^2) G_a(P_j; \frac{\beta}{2M_j u_j''}), \end{aligned} \tag{65}$$

the Gaussian function G_a is defined by $G_a(x;b) = \sqrt{\frac{b}{\pi}} \exp(-bx^2)$, and $u_j'' = u_j \coth u_j$ with $u_j = \beta\hbar\omega_j/2$. We label the results obtained using this formula, which treats the initial distribution of the reaction coordinate and bath quantum mechanically, by QRB.

When the initial distribution of the reaction coordinate and bath is treated classically, we can use Eq. (51) for $W_A^{\alpha'\alpha}$ to obtain

$$\begin{aligned} w_{CRB}^{\alpha\alpha'}(X) = & \frac{P_0}{M_0} \sqrt{\frac{\pi M_0 \beta}{2}} \delta(R_0) G_a(P_0; \frac{\beta}{2M_0}) \frac{\mathcal{F}_{\alpha'\alpha}}{\sum_\alpha e^{-\beta E_\alpha(0)}} \\ & \times \prod_{j=1}^{N} G_a(R_j; \frac{\beta}{2} M_j\omega_j^2) G_a(P_j; \frac{\beta}{2M_j}). \end{aligned} \tag{66}$$

Results obtained using this formula are labeled by CRB.

We used a convenient set of dimensionless coordinates and parameters, which is given in Ref. [40]. The calculations were performed for a bath of $N = 100$ harmonic oscillators with the following values of the parameters: $\omega_{max} = 3$, $\Omega = 0.1$, $\gamma_0 = 0.1$, $a = 0.05$, and $\omega^{\ddagger} = 1$. The simulation scheme for carrying out quantum-classical molecular dynamics has been described in detail earlier [43, 40, 58, 59], so only a few comments about the calculations are needed here. The initial distribution of X for the QRB and CRB results

was sampled from weights determined by Eqs. (65) and (66), respectively. The time evolution of the species variable, $B_W^{\alpha\alpha'}(X,t)$, is determined from constant energy quantum-classical trajectories generated using the sequential short-time propagation algorithm [58].

Results

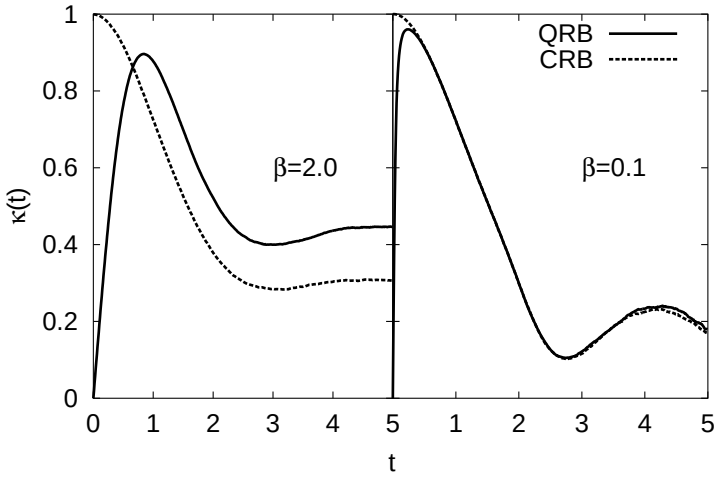

Fig. 2. Comparison between the time-dependent transmission coefficient of the case where the equilibrium structure of the reaction coordinate and bath is treated quantum mechanically (QRB) and that of the case where it is treated classically (CRB). Parameters values: $\beta = 2$ (left), $\beta = 0.1$ (right), $\gamma_0 = 0.1$, $\Omega = 0.1$, and $\xi = 3$.

First, we compare the QRB and CRB rate results for two temperatures in Fig. 2. For high temperatures ($\beta = 0.1$), both the QRB and CRB results are indistinguishable, except at very short times. At $t = 0$, the CRB result for the time-dependent transmission coefficient, $\kappa(t)$, is non-zero and equal to unity, which yields the transition state theory value of the rate constant. The QRB results for the time-dependent transmission coefficient are zero at $t = 0$, which is expected from quantum rate processes [46]. At lower temperatures ($\beta = 2$), where quantum effects are more pronounced, one sees that the QRB formula yields a larger rate constant than does the CRB one. This enhancement of the quantum rate has also been observed in other studies [15, 48, 60].

In Fig. 3, the QRB results for the transmission coefficient κ_{AB}, obtained from the plateau value of $\kappa_{AB}(t)$, are plotted as a function of the Kondo

parameter ξ, which when increased, creates more friction in the bath. As the friction is increased from zero, the rate initially increases to a maximum and then continuously decreases, capturing the well-known turnover behavior [61]. This initial increase at low values of ξ is solely due to quantum effects.

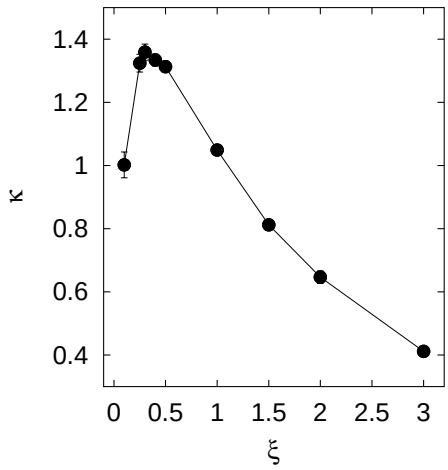

Fig. 3. Transmission coefficient (κ) vs. the Kondo parameter (ξ) for $\beta = 2$,$\gamma_0 = 0.1$, and $\Omega = 0.1$.

4.2 Proton transfer

Model

Proton transfer dynamics plays an important role in many chemical and biological systems. Therefore, an accurate picture of the global dynamics of these systems requires a careful treatment of the proton in the context of its environment. Since these systems are usually too complex and too large to simulate, one can resort to simplified models in order to gain valuable insights. In this connection, we studied a model for a proton transfer reaction (AH-$B \rightleftharpoons A^-$–H^+B) in a hydrogen-bonded complex (AHB) dissolved in a polar solvent. All the details of the model can be found in Ref. [43] and references therein, so we will only mention a few main aspects of it. This model has been used as a benchmark for testing a variety of techniques [62, 63, 64, 65, 66, 67, 68].

The potential energy describing the hydrogen bonding interaction within the complex in the absence of a solvent, which is a function of the protonic

coordinate, models a slightly strongly hydrogen-bonded phenol (A) trimethylamine (B) complex. The parameters which control the strength of the $A-B$ bond were chosen to yield an equilibrium $A-B$ separation of $R_{AB} = 2.7$ Å. For this value of R_{AB}, the potential energy function has two minima, the deeper minimum corresponding to the stable covalent state and the shallower minimum corresponding to the metastable ionic state. We have constrained R_{AB} to be 2.7 Å in our simulations. The AHB complex is dissolved in a solvent composed of 255 polar, nonpolarizable model methyl chloride molecules. The temperature of the system in the simulations performed was approximately 250 K.

The time evolution of the system is determined using quantum-classical Liouville dynamics in which the complex and solvent are treated classically and the proton, quantum mechanically. The Hamiltonian operator, which is partially Wigner transformed over the solvent and A and B groups of the complex, can be found in Ref. [43].

Proton transfer dynamics in polar liquids is usually monitored [69, 70] by the solvent polarization, $\Delta E(R)$,

$$\Delta E(R) = \sum_{i,a} z_a e \left(\frac{1}{|\mathrm{R}_i^a - s|} - \frac{1}{|\mathrm{R}_i^a - s'|} \right), \tag{67}$$

where $z_a e$ ($e = 1.602 \times 10^{-19}$ C) is the charge on solvent atom a, and s and s' are two points within the complex, one at the center of mass and the other displaced by -0.56 Å from the center of mass, respectively, which correspond to the minima of the bare hydrogen bonding potential. The sums run over all solvent molecules i and atoms a. In essence, the solvent polarization is the difference between the solvent electrical potentials at points s and s' and drives the transfer of the proton, making it an ideal reaction coordinate.

In Fig. 4 we see that ΔE tracks the hops of the proton between the reactant/covalent state ($\Delta E \approx 0.005$ eC/Å) and the product/ionic state ($\Delta E \approx 0.0225$ eC/Å). The complex spends more time in the ionic configuration than in the covalent configuration since electrostatic interactions with the polar solvent preferentially stabilize the ionic configuration of the complex. In the absence of the polar solvent, the complex is primarily found in the covalent configuration.

The free energy profiles corresponding to adiabatic evolution on the ground, first and second excited state surfaces, are shown in Fig. 5. The free energy in the ground state has a double-well structure and a single-well structure in the first excited state. The second excited state free energy has a double-well structure with a relatively low barrier. Given the magnitude of the energy gap between the first and second excited state surfaces, the second excited state is not expected to participate strongly in the nonadiabatic quantum-classical dynamics. It is evident from the ground state free energy profile that the minimum of the ionic state is lower in free energy than that of

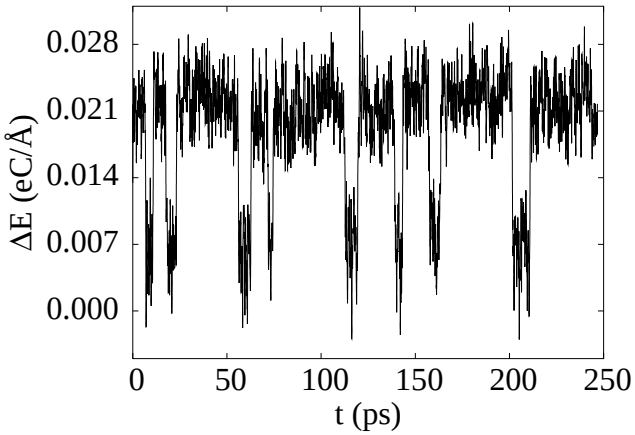

Fig. 4. Time series of the solvent polarization (ΔE) for a ground state adiabatic trajectory.

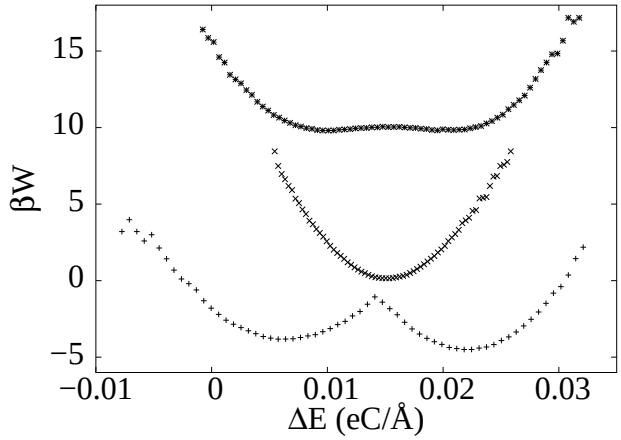

Fig. 5. Free energy (βW) profiles along the ΔE reaction coordinate for the system undergoing ground, first and second excited state adiabatic dynamics.

the covalent state as a result of the stabilizing effect of the polar solvent. The barrier top of the ground state surface is located at $\Delta E^{\ddagger} = 0.0141\ e\mathrm{C/\AA}$.

Since the temperature of the system is fairly high and the dynamics of the solvent and complex atoms can be accurately captured using classical mechanics, a high temperature/classical approximation (analogous to the one which lead to Eq. (51)) is made to obtain a rate expression for this proton transfer reaction that employs $\Delta E(R)$ as the reaction coordinate. Based on the structure of the free energy profiles, we selected the A and B species variables as $\hat{N}_A = \theta(\Delta E(R) - \Delta E^{\ddagger})$ and $\hat{N}_B = \theta(\Delta E^{\ddagger} - \Delta E(R))$, respectively. The

specific form of the diagonal part of the rate coefficient (which turns out to be the major contribution) for this choice of species variables is

$$k_{AB}^{d}(t) = -\frac{1}{n_A^{eq}} \sum_{\alpha} \int dRdP\ \Delta\dot{E}(R) N_B^{\alpha\alpha}(R,P,t) \times \delta(\Delta E(R) - \Delta E^{\ddagger}) \rho_{W_e}^{\alpha\alpha}\ , \tag{68}$$

where the equilibrium fraction of species A is

$$n_A^{eq} = \int d\Delta E'\ \theta(\Delta E(R) - \Delta E^{\ddagger}) e^{-\beta W(\Delta E')} P_u, \tag{69}$$

and the time derivative of the solvent polarization can be rewritten as $\Delta\dot{E}(R) = \frac{P}{M} \cdot \nabla_R \Delta E(R)$. The canonical equilibrium distribution is given by $\rho_{W_e}^{\alpha\alpha} = Z_0^{-1} e^{-\beta H_W^{\alpha}}$, with $Z_0 = \sum_{\alpha} \int dRdP\ e^{-\beta H_W^{\alpha}}$.

Equation (68) provides a well-defined formula involving initial sampling from the barrier top $\Delta E = \Delta E^{\ddagger}$. In addition, quantum-classical time evolution of $N_B^{\alpha\alpha}(R,P,t)$ must be carried out to compute the reaction rate.

Results

In Fig. 6, we present results for the time-dependent rate coefficient which were obtained from an average over 16000 trajectories. As expected from the high temperature form of the rate coefficient, we see that it falls quickly from its initial transition state theory value in a few tenths of a picosecond to a plateau from which the rate constant can be extracted. The decrease in the rate coefficient from its transition state theory value is due to recrossing by the trajectory of the barrier top before the system reaches a stable state. The value of k_{AB} obtained from the plateau is $k_{AB} = 0.013$ ps^{-1}. This result is 32% lower than the adiabatic result, indicating a significant nonadiabatic quantum correction.

5 Concluding Remarks

The theory presented in this chapter shows how chemical reaction rates can be computed from time correlation function expressions that retain the quantum equilibrium structure of the system and employ a quantum-classical description of the dynamics of the species variables. Thus, the computational method combines a surface-hopping dynamics based on the quantum-classical Liouville equation, with initial sampling from a quantum equilibrium distribution. As such, the method differs from conventional surface-hopping schemes for reactive quantum-classical dynamics, both in the nature of the time evolution of operators and in the way the trajectories are sampled to compute the reaction rate.

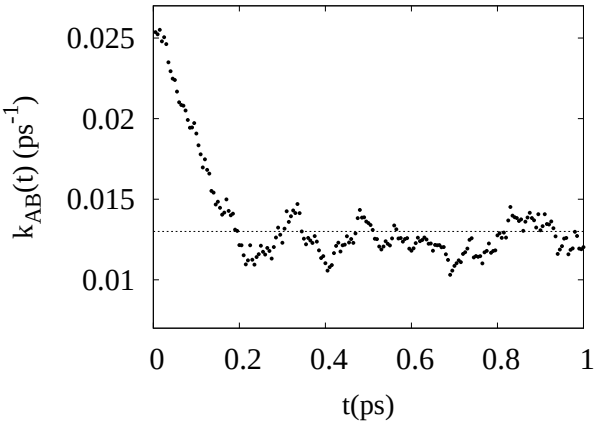

Fig. 6. The rate coefficient, $k_{AB}(t)$, as a function of time. The dotted line indicates the plateau value k_{AB}.

The simulation results reported above utilized various approximate analytical expressions for the spectral density function that describes the quantum equilibrium structure. In some circumstances, especially for low temperatures, effects arising from the quantum equilibrium structure lead to important modifications of the reaction rate. To treat more general and complex molecular systems one could resort to numerical schemes for computing the equilibrium structure, similar to those based on the initial value representation [68, 71, 72] and linearization techniques [50, 73, 74, 75].

Different formulas for the time-dependent rate coefficient can be derived within this framework using other choices of the reaction coordinate and chemical species variables. These should allow one to effectively capture quantum effects in a variety of chemical rate processes occurring within a wide range of temperatures and in complex condensed phase environments.

References

1. A. Kohen, J. P. Klinman: Acc. Chem. Res. **31**, 397 (1998)
2. J. Lobaugh, G. A. Voth: J. Chem. Phys. **104**, 2056 (1996)
3. D. Marx, M. E. Tuckerman, J. Hutter, M. Parrinello: Nature **397**, 601 (1999)
4. T. Yamamoto: J. Chem. Phys. **33**, 281 (1960)
5. K. Thompson, N. Makri: J. Chem. Phys. **110**, 1343 (1999)
6. N. Makri: J. Phys. Chem. B **103**, 2823 (1999)
7. N. Makri, W. H. Miller: J. Chem. Phys. **89**, 2170 (1988)
8. C. H. Mak, D. Chandler: Phys. Rev. A **44**, 2352 (1991)
9. J. T. Stockburger, H. Grabert: Chem. Phys. **268**, 249 (2001)
10. J. S. Shao, C. Zerbe, P. Hanggi: Chem. Phys. **235**, 81 (1998)
11. E. Geva, Q. Shi, G. A. Voth: J. Chem. Phys. **115**, 9209 (2001)

12. R. I. Cukier, J. J. Zhu: J. Phys. Chem. **101**, 7180 (1997); R. I. Cukier: J. Chem. Phys. **88**, 5594 (1988)
13. D.R. Reichman, E. Rabani: Phys. Rev. Lett. **87**, 265702 (2001)
14. E. Rabani, D.R. Reichman: J. Chem. Phys. **120**, 1458 (2004)
15. H.B. Wang, X. Sun, W.H. Miller: J. Chem. Phys. **108**, 9726 (1998)
16. X. Sun, H.B. Wang, W.H. Miller: J. Chem. Phys. **109**, 7064 (1998)
17. X. Sun, H.B. Wang, and W.H. Miller: J. Chem. Phys. **109**, 4190 (1998)
18. X. Sun and W.H. Miller: J. Chem. Phys. **110**, 6635 (1999)
19. W.H. Miller: J. Phys. Chem. A **105**, 2942 (2001)
20. M. Thoss and H.B. Wang: Annu. Rev. Phys. Chem. **55**, 299 (2004)
21. K.G. Kay: Annu. Rev. Phys. Chem. **56**, 255 (2005)
22. M. A. Sepulveda, F. Grossmann: Adv. Chem. Phys. **96**, 191 (1996)
23. S. Bonella and D. F. Coker: J. Chem. Phys. **122**, 194102 (2005)
24. S. Bonella, D. Montemayor, D.F. Coker: Proc. Natl. Acad. Sci. **102**, 6715 (2005)
25. A. A. Neufeld: J. Chem. Phys. **122**, 164111 (2005)
26. J.C. Tully: J. Chem. Phys. **93**, 1061 (1990)
27. S. Hammes-Schiffer and J.C. Tully: J. Chem. Phys. **101**, 4657 (1994)
28. D.F. Coker, L. Xiao: J. Chem. Phys. **102**, 496 (1995)
29. F. Webster, E.T. Wang, P.J. Rossky, R.A. Friesner: J. Chem. Phys. **100**, 4835 (1994)
30. A.W. Jasper, S.N. Stechmann, D.G. Truhlar: J. Chem. Phys. **116**, 5424 (2002)
31. H. Wang, M. Thoss: J. Chem. Phys. **119**, 1289 (2003)
32. H. Wang, M. Thoss: Chem. Phys. Lett. **389**, 43 (2004)
33. I. V. Aleksandrov: Z. Naturforsch. **36**, 902 (1981)
34. A. Donoso, C.C. Martens: J. Phys. Chem. A **102**, 4291 (1998)
35. V. I. Gerasimenko: Theor. Math. Phys. **50**, 49 (1982)
36. I. Horenko, C. Salzmann, B. Schmidt, C. Schutte: J. Chem. Phys. **117**, 11075 (2002)
37. R. Kapral, G. Ciccotti: J. Chem. Phys. **110**, 8919 (1999)
38. C. Wan, J. Schofield: J. Chem. Phys. **113**, 7047 (2000)
39. S. Nielsen, R. Kapral, G. Ciccotti: J. Chem. Phys. **115**, 5805 (2001)
40. A. Sergi, R. Kapral: J. Chem. Phys. **118**, 8566 (2003)
41. J.L. Liao, E. Pollak: J. Chem. Phys. **116**, 2718 (2002)
42. A. Sergi, R. Kapral: J. Chem. Phys. **119**, 12776 (2003)
43. G. Hanna, R. Kapral: J. Chem. Phys. **122**, 244505 (2005)
44. A. Sergi, R. Kapral: J. Chem. Phys. **121**, 7565 (2004)
45. H. Kim, R. Kapral: J. Chem. Phys. **122**, 214105 (2005)
46. R. Kapral, S. Consta, L. McWhirter: Chemical rate laws and rate constants. In: *Classical and Quantum Dynamics in Condensed Phase Simulations*, ed by B. J. Berne, G. Ciccotti, D. F. Coker (World Scientific Singapore 1998) pp 583–617
47. H. Kim, R. Kapral: J. Chem. Phys. **123**, 194108 (2005)
48. M. Topaler and N. Makri: J. Chem. Phys. **101**, 7500 (1994)
49. H. Kim, P.J. Rossky: J. Phys. Chem. B **106**, 8240 (2002)
50. J.A. Poulsen, G. Nyman, P.J. Rossky: J. Chem. Phys. **119**, 12179 (2003)
51. H. A. Kramers: Physica **6**, 284 (1940)
52. E. Pollak, J.L. Liao: J. Chem. Phys. **108**, 2733 (1998)
53. J.S. Shao, J.L. Liao, E. Pollak: J. Chem. Phys. **108**, 9711 (1998)
54. G.A. Voth, D. Chandler, W.H. Miller: J. Chem. Phys. **91**, 7749 (1989)
55. P.G. Wolynes: Phys. Rev. Lett. **47**, 968 (1981)

56. N. Makri, K. Thompson: Chem. Phys. Lett. **291**, 101 (1998); K. Thompson, N. Makri: J. Chem. Phys. **110**, 1343 (1999); N. Makri: J. Phys. Chem. B **103**, 2823 (1999)
57. D. MacKernan, R. Kapral, G. Ciccotti: J. Chem. Phys. **116**, 2346 (2002)
58. D. MacKernan, R. Kapral, G. Ciccotti: J. Phys.: Condens. Matter **14**, 9069 (2002)
59. A. Sergi, D. MacKernan, G. Ciccotti, R. Kapral: Theor. Chem. Acc. **110**, 49 (2003)
60. E. Rabani, G. Krilov, B.J. Berne: J. Chem. Phys. **112**, 2605 (2000)
61. P. Hanggi, P. Talkner, M. Borkovec: Rev. Mod. Phys. **62**, 251 (1990)
62. H. Azzouz, D. C. Borgis: J. Chem. Phys. **98**, 7361 (1993)
63. S. Hammes-Schiffer, J. C. Tully: J. Chem. Phys. **101**, 4657 (1994)
64. R. P. McRae, G. K. Schenter, B. C. Garrett, Z. Svetlicic, D. G. Truhlar: J. Chem. Phys. **115**, 8460 (2001)
65. D. Antoniou, S. D. Schwartz: J. Chem. Phys. **110**, 465 (1999)
66. D. Antoniou, S. D. Schwartz: J. Chem. Phys. **110**, 7359 (1999)
67. S. Y. Kim, S. Hammes-Schiffer: J. Chem. Phys. **119**, 4389 (2003)
68. T. Yamamoto, W. H. Miller: J. Chem. Phys. **122**, 044106 (2005)
69. P. M. Kiefer, J. T. Hynes: Solid State Ionics **168**, 219 (2004)
70. D. Laria, G. Ciccotti, M. Ferrario, R. Kapral: J. Chem. Phys. **97**, 378 (1992)
71. T. Yamamoto, W.H. Miller: J. Chem. Phys. **118**, 2135 (2003)
72. Y. Zhao, T. Yamamoto, W.H. Miller: J. Chem. Phys. **120**, 3100 (2004)
73. J. A. Poulsen, G. Nyman, P. J. Rossky: J. Phys. Chem. A **108**, 8743 (2004)
74. Q. Shi, E. Geva: J. Chem. Phys. **118**, 8173 (2003)
75. Q. Shi, E. Geva: J. Chem. Phys. **120**, 10647 (2004)